Electrofriction and Dynamic Stern Layers at Planar Charged Surfaces

R. R. Netz

Sektion Physik, LMU Munich, Theresienstrasse 37, 80333 Munich, Germany

(Received 14 May 2003; published 25 September 2003)

Using dynamic simulations, the electrophoretic mobility of counterions at a substrate with fixed or mobile surface charges under the action of a lateral electric field is studied. The lateral charge inhomogeneity and corrugation of the substrate is taken into account. Because of the pronounced electrofriction between counterions and surface ions, a large fraction of counterions is practically immobilized for highly charged substrates. This explains the experimentally observed saturation of the electrophoretic mobility of charged particles in the limit of high surface charge density.

DOI: 10.1103/PhysRevLett.91.138101 PACS numbers: 87.15.–v, 68.08.–p, 82.45.–h

Charged surfaces are neutralized by a diffuse cloud of oppositely charged ions which extends a certain distance into the aqueous half-space. Electrokinetic methods give useful information on the structure of this electric double layer [1,2]. When a charged macroscopic particle is subjected to an electric field, it migrates at constant speed; this process is called electrophoresis. If, on the other hand, the particle is held fixed, the diffuse counterion layer will move and thereby drag the solvent along; this process is called electro-osmosis. A simple description is possible for a *planar* charged substrate with a tangential electric field E along the x direction (see Fig. 1). The Stokes equation (valid for small Reynolds numbers, i.e., small particles and moderate velocities [2]) describes the stationary solvent velocity v_x along x as a function of the distance z from the substrate as $\eta d^2 v_x(z)/dz^2 = -\rho_e(z)E$, where η is the solvent viscosity and ρ_e is the local charge density in the solvent. Inserting the Poisson equation leads to $\eta d^2 v_x(z)/dz^2 = \varepsilon E d^2\psi(z)/dz^2$, where ε is the dielectric constant and ψ is the electrostatic potential. Integrating twice, one finally obtains the celebrated Helmholtz-Smoluchowski (HS) equation, $\eta v_x(\infty) = -\varepsilon E \psi_s$, which relates the solvent flow far away from the substrate, $v_x(\infty)$, to the so-called *Zeta potential*, $\psi_s = \psi(z_s)$, i.e., the electrostatic potential at the surface of shear z_s up to which the fluid stays at rest. Extensions of the above arguments to the cases of inhomogeneous charge distributions [3] and perpendicular electric fields [4] exist.

In order to match Zeta potentials (obtained from mobility measurements via the HS equation) with surface potentials derived from the actual charge of highly charged particles, a large fraction of counterions has to be assumed to lie within the surface of shear [1,2,5]. This layer of counterions is customarily associated with the Stern layer (initially introduced to account for ions *statically* surface adsorbed by nonelectrostatic forces [6]). Alternative explanations involve a spatially varying viscosity or dielectric constant close to the substrate [1,7]. The situation is complicated by the fact that conduction measurements indicate that a large fraction of ions below the surface of shear (where the solvent stagnates) is fairly mobile and contributes to the electric current [8]. These concepts introduce a number of adjustable and hard to directly measurable parameters (in that respect it is interesting to note that the concept of a no-slip shear surface has been critically examined for uncharged simple liquids at large shear [9]). Obviously, there is an intricate interplay between solvent viscosity effects (embodied by the concept of the shear surface within HS theory) and friction effects between counterions and more or less localized and protruding surface charges (excluded in all standard treatments by the assumption of lateral substrate homogeneity). The present paper is a first step towards a microscopic understanding of this friction (including effects far from equilibrium, i.e., large electric fields). We use dynamic simulation methods and consider a surface made up of charged, hard spheres (which are either fixed or can move in the electric field). In the simulations, we neglect hydrodynamic interactions and concentrate on the direct electrostatic friction between surface ions and counterions; hydrodynamic effects are taken into account at the end by adapting the HS equation. We introduce a dynamic interpretation of the Stern layer, which is defined to comprise all ions that are *dynamically bound to the substrate*. For highly charged surfaces, more and more counterions become immobilized, in accord with measured Zeta potentials [5].

In the simulations we consider a two-dimensional layer of N charged spheres of valency q and diameter a (at $z = 0$), together with N oppositely charged counterions of the same valency and diameter, which are confined to the upper half-space ($z > 0$) in a cubic simulation

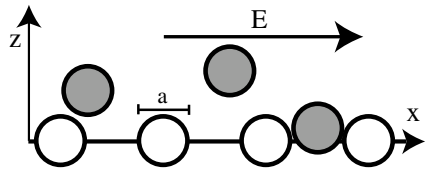

FIG. 1. In the simulations, a two-dimensional layer of surface ions (which can be mobile or fixed) is in contact with oppositely charged counterions of the same diameter a and valency q. The electric field acts laterally.

box of length L (see Fig. 1). The density of surface ions is $\rho_s = N/L^2$. From the position Langevin equation, the velocity of the ith particle at time t follows as

$$\dot{\mathbf{r}}_i(t) = -\mu_0 \nabla_{\mathbf{r}_i} U(t) + \mu_0 q e s_i \mathbf{E} + \boldsymbol{\xi}_i(t), \qquad (1)$$

where μ_0 is the bare particle mobility, U is the potential energy, $\mathbf{E}$ the external electric field, $s_i = \pm 1$ for surface ions/counterions, and $\boldsymbol{\xi}_i$ is a vectorial random force acting on particle i. The random force is correlated according to $\langle \boldsymbol{\xi}_i(t) \cdot \boldsymbol{\xi}_j(t') \rangle = 6 k_B T \mu_0 \delta(t - t') \delta_{ij}$. In the simulations, we discretize Eq. (1) with a time step Δ and rescale all lengths by the ion diameter a according to $\tilde{\mathbf{r}}_i = \mathbf{r}_i/a$. The iterative Langevin equation in terms of the discrete time variable $n = t/\Delta$ now reads

$$\tilde{\mathbf{r}}_i(n+1) = \tilde{\mathbf{r}}_i(n) - \tilde{\mu}_0 \nabla_{\tilde{\mathbf{r}}_i} \tilde{U}(n) + \tilde{\mu}_0 s_i \tilde{\mathbf{E}} + \sqrt{6 \tilde{\mu}_0} \tilde{\boldsymbol{\xi}}_i(n),$$

where $\tilde{U} = U/k_B T$ is the dimensionless potential energy, $\tilde{\mathbf{E}} = qea\mathbf{E}/k_B T$ the rescaled electric field, and the rescaled random force has variance unity, $\langle \tilde{\boldsymbol{\xi}}_i(m) \cdot \tilde{\boldsymbol{\xi}}_j(n) \rangle = \delta_{mn} \delta_{ij}$. The only dynamic parameter remaining is the rescaled mobility $\tilde{\mu}_0 = \Delta \mu_0 k_B T/a^2$ which is the diffusion constant in units of the particle diameter a and time step Δ. We chose $\tilde{\mu}_0 = 0.0005$ as a compromise between efficiency and accuracy. The potential energy has two contributions, $\tilde{U} = \tilde{U}_c + \tilde{U}_{LJ}$. The Coulombic part is

$$\tilde{U}_c = \zeta \sum_{i<j} \frac{s_i s_j}{|\tilde{\mathbf{r}}_i - \tilde{\mathbf{r}}_j|}, \qquad (2)$$

where $\zeta = q^2 \ell_B/a$ is the Coulomb parameter and measures the ratio of the Coulomb interaction and the thermal energy at the minimal distance a [$\ell_B = e^2/[4\pi\varepsilon k_B T]$ is the Bjerrum length, in water, $\ell_B \approx 0.7$ nm]. Collapse of counterions and surface ions is prevented by a truncated Lennard-Jones term acting between all particles,

$$\tilde{U}_{\mathrm{LJ}} = \epsilon \sum_{i<j} \left(\frac{1}{(\tilde{\mathbf{r}}_i - \tilde{\mathbf{r}}_j)^{12}} - \frac{2}{(\tilde{\mathbf{r}}_i - \tilde{\mathbf{r}}_j)^6} + 1 \right), \qquad (3)$$

used for separation $|\tilde{\mathbf{r}}_i - \tilde{\mathbf{r}}_j| < 1$ only with an energy parameter $\epsilon = 1$. Boundary effects are minimized by using minimal image boundary conditions. Equilibration takes roughly 10^6 time steps; simulations were run for typically 10^7 time steps with $N = 50$ to 200 particles with no detectable finite-size effects.

The model we consider includes the combined effects of discrete surface charges, surface corrugations, and counterion excluded volume, which are all neglected in the classical mean-field approaches. To clarify the static case, we show in Fig. 2 laterally averaged counterion density profiles for fixed Coulomb strength $\zeta = 2.5$ and various surface-ion densities, together with the mean-field (MF) prediction for the laterally homogeneous case [10], which reads in normalized form $\rho(z)/\rho_s = \mu^{-1}/(1 + z/\mu)^2$. The Gouy-Chapman length $\mu = a/(2\pi\zeta a^2 \rho_s)$ is a measure of the decay length of the profiles. For small densities, Fig. 2(a), the measured profiles agree quite well with the MF predictions, as expected, since the Gouy-Chapman length is larger than the lateral surface-ion separation and the charge modulation and hard-core repulsion matter little. However, even for the smallest density considered (open squares), there are some deviations in the distance range $z/a < 1$ which we attribute to the hard-core repulsion between surface ions and counterions [11]. For the larger surface densities in Fig. 2(b), the deviations become more pronounced (simply shifting the MF profiles does not lead to satisfactory agreement). For $\rho_s a^2 = 0.5$ (open diamonds), some counterions still reach the surface at $z = 0$, but the profile is considerably shifted to larger values of z due to the impenetrability of surface ions and counterions. Finally, for $\rho_s a^2 = 2$ (filled triangles), the surface ions form an impenetrable but highly corrugated layer, and the counterion profile is shifted almost by an ion diameter outwards (and a second layer of counterions forms). These results remind us that in experimental systems a number of effects are present which make comparison with theories based on laterally homogeneous charge distributions difficult. The traditional concept of a statically defined Stern-layer beyond which MF profiles are recovered is therefore highly ambiguous. As a side remark, the coupling constant $\Xi = 2\pi\rho_s a^2 \zeta^2$ (which measures deviations from MF theory due to fluctuations and correlations) is for the data in Fig. 2(b) in a range where deviations from MF theory are becoming noticeable for the smeared-out case [12] but are totally overwhelmed by the more drastic effects illustrated in Fig. 2.

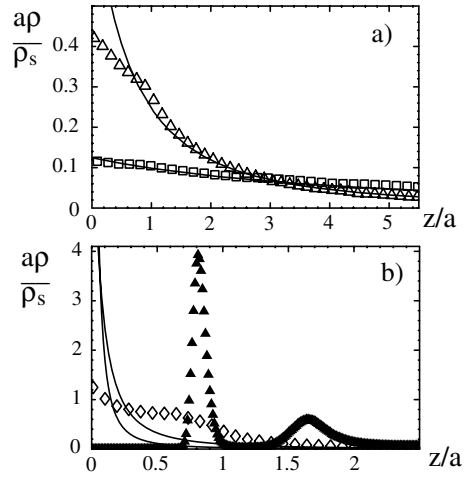

FIG. 2. Laterally averaged counterion-density profiles for Coulomb coupling $\zeta = 2.5$ for zero electric field as a function of the rescaled distance from the surface (surface ions are fixed on a square lattice). Shown are results for surface ion densities (a) $\rho_s a^2 = 0.0079$ (open squares) and $\rho_s a^2 = 0.05$ (open triangles), (b) $\rho_s a^2 = 0.5$ (open diamonds) and $\rho_s a^2 = 2$ (filled triangles), together with the mean-field predictions for the laterally homogeneous case (solid lines).

In Fig. 3, we plot the mean electrophoretic counterion mobility, which is an average over all counterions according to $\tilde{\mu} = \sum_{i=1}^{N} (\tilde{\mathbf{r}}_i(n+1) - \tilde{\mathbf{r}}_i(n))/(N\tilde{E})$ and is equivalent to the conductivity. The mobility $\tilde{\mu}$ divided

by the bare mobility $\tilde{\mu}_0$ reaches unity for vanishing interactions between surface ions and counterions and also in the case of a laterally homogeneous substrate. Indeed, for $\zeta = 0.5$ (open diamonds), the mobility for mobile and fixed surface ions in Figs. 3(a) and 3(b) is close to the maximal value of unity. Experimentally, the minimal distance between oppositely charged dehydrated ions is 2.5 Å; for monovalent ions a typical value for the Coulomb parameter thus is $\zeta = 3$. For elevated densities of the order of $\rho_s a^2 \approx 0.5$, reached in highly charged surfactant layers or minerals, our results indicate for $\zeta = 3$ a mean mobility of roughly one-half. This decrease in electrophoretic mobility is solely caused by the electrostatic friction between surface ions and counterions and has not been included in previous theoretical attempts to explain the observed decrease of electrophoretic mobility of highly charged particles. In order to be able to combine hydrodynamic effects (as embodied in the HS theory) and electrofriction, we have to understand the microscopic structure of the counterion layer in more detail.

In Fig. 4, we show ion snapshots both for mobile and fixed surface ions for surface-ion density $\rho_s a^2 = 0.5$ and coupling $\zeta = 2.5$ and different field strengths. For small fields, the counterions penetrate into the surface-ion layer. As the electric field is increased, counterions lift off from the surface ions and form a "floating layer." This is paralleled by the mobility in Fig. 3(c) which increases as a function of the field [a field of $\tilde{E} = 0.4$ as used in Figs. 3(a) and 3(b) corresponds to the quasistatic limit]. One notes a pronounced mobility difference between the mobile and fixed surface-ion cases, which might help to rationalize the observed Zeta-potential differences between surfaces with stiff and rather flexible or protruding surface groups [1]. Likewise, it seems that a strong applied field might preempt the demixing transition predicted for highly charged mobile surface-ion layers [13].

In Figs. 5(a) and 5(b), the corresponding counterion density profiles are shown for the mobile and fixed surface-ion case. As already seen in the snapshots, the density profiles shift to larger distances in the z direction for increasing field strength. By doing this, the counterions avoid being trapped within the surface-ion layer, and the conduction is maximized (though hydrodynamic interactions will certainly play a role at such elevated field strengths). In Fig. 5(c), the corresponding counterion mobility profile is shown for the fixed surface-ion case [the mean mobility in Fig. 3 is the integrated product of the density and mobility profiles in Figs. 5(b) and 5(c)]. For the smallest field considered, $\tilde{E} = 1$ (open diamonds), which belongs to the linear quasistatic regime, the mobility is highly reduced for distances below roughly $z/a = 1$, which is plausible since in this distance range surface ions and counterions experience strong excluded-volume interactions. The maximal mobility of $\tilde{\mu}/\tilde{\mu}_0 = 1$ is reached quickly for larger separations from the surface. For larger fields, the crossover in the mobility profiles moves closer to the surface and, since the density at the

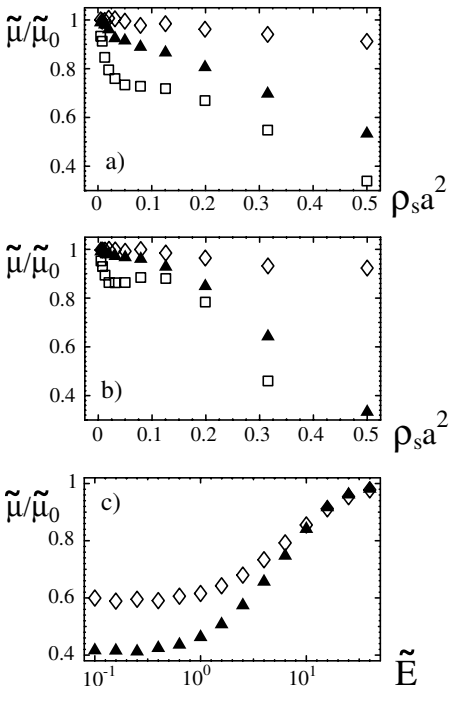

FIG. 3. Averaged electrophoretic counterion mobility for Coulomb parameters $\zeta = 0.5$ (open diamonds), $\zeta = 3$ (filled triangles), and $\zeta = 5.5$ (open squares) in a constant lateral field $\tilde{E} = 0.4$ as a function of the surface ion density for (a) mobile surface ions and (b) surface ions fixed on a square lattice. (c) Electrophoretic counterion mobility for mobile (open diamonds) and fixed surface ions (filled triangles) at surface-ion density $\rho_s a^2 = 0.5$ and Coulomb coupling $\zeta = 2.5$ as a function of the reduced electric field.

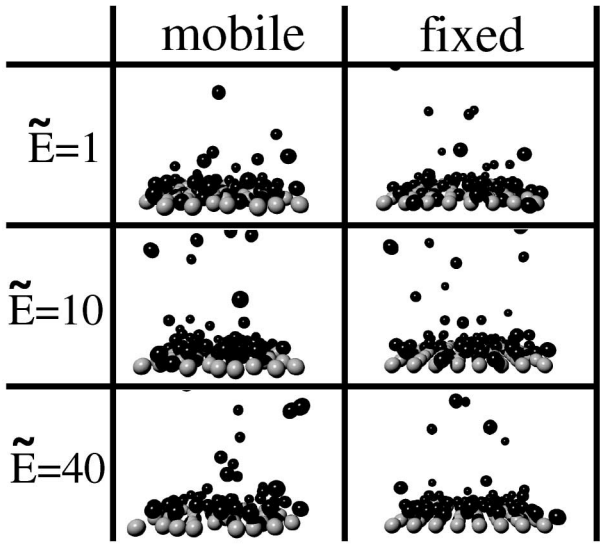

FIG. 4. Snapshots of ion configurations for a surface density $\rho_s a^2 = 0.5$ and Coulomb coupling $\zeta = 2.5$ for different field strengths. In the left column, the surface ions are mobile; in the right column, the surface ions are fixed on a square lattice. The field moves counterions from the right to the left (and mobile surface ions in the opposite direction).

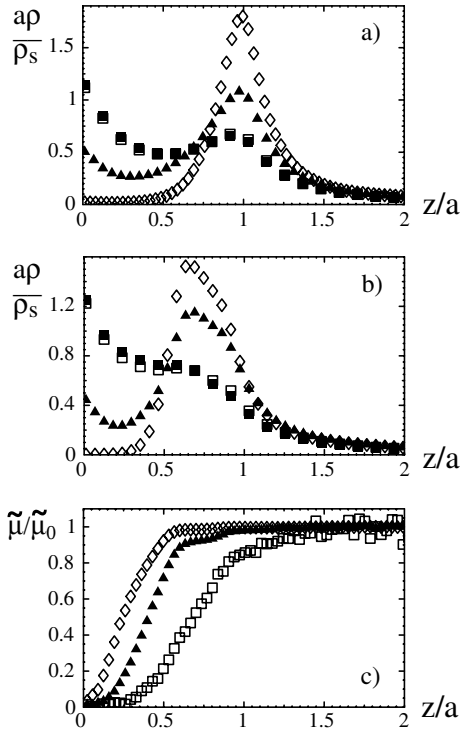

FIG. 5. Counterion density profiles for fixed Coulomb coupling $\zeta = 2.5$ and surface ion density $\rho_s a^2 = 0.5$ for different electric field strengths $\tilde{E} = 0$ (filled squares), $\tilde{E} = 1$ (open squares), $\tilde{E} = 10$ (filled triangles), and $\tilde{E} = 40$ (open diamonds) for (a) mobile and (b) fixed surface ions. (c) Shown are the counterion mobility profiles for fixed surface ions for three different electric field strengths; same notation as in (b).

wall decreases, the fraction of immobile counterions goes drastically down [and the average reduced mobility reaches unity quickly for elevated fields, see Fig. 3(c)]. These results suggest how to include frictional effects within the HS theory: Since the decrease of the mean electrophoretic mobility is caused by a fairly localized layer of immobilized counterions, the relative mobility $\tilde{\mu}/\tilde{\mu}_0$ can be interpreted as the fraction of mobile ions, or, in other words, the fraction of counterions that is not located within the stagnant Stern layer (according to a *dynamical definition of the Stern layer* which is unambiguous and connects to the experimentally relevant Zeta potential). This amounts to replacing the profiles in Fig. 5(c) by step profiles. Furthermore assuming the surface of shear to coincide with the Stern-layer surface, the HS equation is valid provided the Zeta potential ψ_s is calculated for a surface charge *reduced by the immobilized counterions*. Our results for the mean counterion mobility (i.e., the fraction of mobile counterions) in Figs. 3(a) and 3(b) show that the electrophoretic mobility or Zeta potential is predicted to decrease drastically as the charge density increases, without the need to invoke modified surface viscosities or dielectric constants [1,7] (which clearly play a role, though maybe less prominently as believed). Experimentally, the fraction of mobile counterions, inferred from mobility measurements of polystyrene lattices at low salt, was found to be 1.05, 0.83, and 0.71 for charge densities $\rho_s \ell_B^2 = 0.154$, 0.31, and 0.34, respectively [5], in qualitative agreement with our results [see Fig. 3(b)].

A reduced electric field $\tilde{E} = 1$, approximately where the crossover between the linear and the dissipation-dominated far-from-equilibrium regime starts, corresponds for an ion diameter $a = 0.25$ nm and monovalent ions ($q = 1$) to a field of $E \simeq 1 \times 10^8$ V/m which is beyond experimental field strengths. This shows that nonlinear effects are unimportant in electrophoretic experiments using substrates with corrugations on the atomic scale (and $q = 1$). On the other hand, assuming a modulation wavelength of $a = 5$ μm and a macroion valency of $q = 200$ gives for a reduced value of $\tilde{E} = 1$ a field strength of $E \simeq 100$ V/m which is a very moderate value. Modifications of ion-distribution functions at structured substrates in far-from-equilibrium situations should thus be easily observable in microstructured electrophoretic chambers and using macroions (DNA molecules or charged proteins and colloids).

This work was financially supported by Deutsche Forschungsgemeinschaft (DFG, German-French Network) and the Fonds der Chemischen Industrie.

[1] J. Lyklema, *Fundamentals of Interface and Colloid Science* (Academic, New York, 1995).
[2] R. J. Hunter, *Foundations of Colloid Science* (Oxford University Press, Oxford, 2001).
[3] A. Ajdari, Phys. Rev. Lett. **75**, 755 (1995).
[4] R. Golestanian, Europhys. Lett. **52**, 47 (2000).
[5] B. R. Midmore, G.V. Pratt, and T. M. Herrington, J. Colloid Interface Sci. **184**, 170 (1996).
[6] O. Stern, Z. Elektrochem. **30**, 508 (1924); R. Podgornik, J. Chem. Phys. **91**, 5840 (1989); O. Spalla and L. Belloni, J. Chem. Phys. **95**, 7689 (1991); M. Boström, D. R. M. Williams, and B.W. Ninham, Phys. Rev. Lett. **87**, 168103 (2001).
[7] J. Lyklema and J.T.G. Overbeek, J. Colloid Sci. **15**, 501 (1961).
[8] J. Lyklema and M. Minor, Colloids Surf. A **140**, 33 (1998).
[9] V. S. J. Craig, C. Neto, and D. R. M. Williams, Phys. Rev. Lett. **87**, 054504 (2001); Y. Zhu and S. Granick, Phys. Rev. Lett. **88**, 106102 (2002).
[10] G. Gouy, J. Phys. **IX**, 457 (1910); D. L. Chapman, Philos. Mag. **25**, 475 (1913).
[11] Charge modulation without hard-core repulsion increases the surface counterion density; see A. G. Moreira and R. R. Netz, Europhys. Lett. **57**, 911 (2002); D. B. Lukatsky, S. A. Safran, A.W.C. Lau, and P. Pincus, *ibid.* **58**, 785 (2002).
[12] A. G. Moreira and R. R. Netz, Europhys. Lett. **52**, 705 (2000).
[13] A.W.C. Lau, D. B. Lukatsky, P. Pincus, and S. A. Safran, Phys. Rev. E **65**, 051502 (2002).